

Dynamically assisted tunneling in the impulse regime

Christian Kohlfürst,¹ Friedemann Queisser,^{1,2} and Ralf Schützhold^{1,2}

¹*Helmholtz-Zentrum Dresden-Rossendorf, Bautzner Landstraße 400, 01328 Dresden, Germany,*

²*Institut für Theoretische Physik, Technische Universität Dresden, 01062 Dresden, Germany,*

(Dated: February 16, 2021)

We study the enhancement of tunneling through a potential barrier $V(x)$ by a time-dependent electric field with special emphasis on pulse-shaped vector potentials such as $A_x(t) = A_0/\cosh^2(\omega t)$. In addition to the known effects of pre-acceleration and potential deformation already present in the adiabatic regime, as well as energy mixing in analogy to the Franz-Keldysh effect in the non-adiabatic (impulse) regime, the pulse $A_x(t)$ can enhance tunneling by “pushing” part of the wave-function out of the rear end of the barrier. Besides the natural applications in condensed matter and atomic physics, these findings could be relevant for nuclear fusion, where pulses $A_x(t)$ with $\omega = 1$ keV and peak field strengths of 10^{16} V/m might enhance tunneling rates significantly.

I. INTRODUCTION

One of the most striking differences between classical and quantum mechanics is the tunnel effect. Even though this phenomenon cannot be directly observed with the naked eye [1], it plays an important role in many areas of physics and across a wide variety of length scales – including ultra-cold atoms in optical lattices on the micrometer scale (see, e.g., [2]), and ranging down to nuclear physics in the femtometer regime [3, 4]. However, although tunneling is usually taught in the first lecture course on quantum mechanics, our intuition and understanding, especially regarding time-dependent scenarios, is still far from complete [5].

In order to be more specific, let us consider the one-dimensional Schrödinger equation describing a particle with energy E and mass m incident on a potential barrier $V(x)$. Then, using the standard WKB approximation, we may derive the tunneling probability \mathcal{P} (or, more precisely, its exponential contribution) and arrive at the following famous expression, which, as Sidney Coleman [6] puts it, “every child knows” ($\hbar = 1$)

$$\mathcal{P} \sim e^{-2\mathfrak{S}_E} = \exp \left\{ -2 \int_{x_{\text{in}}^E}^{x_{\text{out}}^E} dx \sqrt{2m[V(x) - E]} \right\}. \quad (1)$$

Here x_{in}^E and x_{out}^E are the classical turning points with $V(x_{\text{in}}^E) = V(x_{\text{out}}^E) = E$ (assuming that there are only two of them). Alternatively, one could employ the instanton picture where \mathfrak{S}_E denotes the Euclidean action [6].

Adding a temporal dependence $V(t, x)$, however, the situation becomes far more complex. Only in certain limiting cases, such as slowly varying or rapidly oscillating potentials $V(t, x)$, simple expressions similar to Eq. (1) can be derived via the quasi-static or the time-averaged potential approximation.

In the following, we do not consider the general case $V(t, x)$, but we focus on the simpler (yet non-trivial) scenario of a static potential barrier superimposed by a purely time-dependent electric field. In the Coulomb gauge, this case can be represented by a space-time dependent potential $V(t, x) = V_0(x) + xV_1'(t)$, but we find

it more convenient to represent the electric field via the vector potential $A(t)$ in the temporal gauge.

In order to understand the impact of the additional electric field on the tunneling probability (1) of a charged particle, let us try to separate the phases of the temporal evolution:

First, even before hitting the barrier, the electric field can accelerate (or decelerate) the particle which effectively increases (or decreases) the energy E and changes the classical turning points x_{in}^E and x_{out}^E . This effect already occurs in the adiabatic regime of slowly varying electric fields.

In contrast, the time-dependence of $A(t)$ can induce additional phenomena in the non-adiabatic (impulse) regime. Thus, as the second effect, the energy E is no longer conserved due to this temporal variation, i.e., it can effectively shift the energy up or down. Assuming a harmonic oscillation $A(t) = A_0 \sin(\omega t)$, for example, this effect can be understood in the Floquet picture [7] where we get side-bands with effective energies $E \pm n\hbar\omega$ (in analogy to the Franz-Keldysh effect [8, 9].) In view of the exponential decay of the wave-function inside the barrier, this effect can typically most efficiently enhance the tunneling rate when the mixing occurs near the front end x_{in}^E of the barrier.

Third, the electric field effectively deforms the barrier and thereby changes the tunneling probability (1). Similar to the first contribution (pre-acceleration) and in distinction to the second (energy mixing), this effect already occurs in the adiabatic regime.

Finally, the time-dependent electric field may enhance tunneling by effectively “pushing” part of the wave-function out of the rear end x_{out}^E of the barrier in the non-adiabatic (impulse) regime. (Reversing the electric field would then suppress tunneling by “pulling” it back into the barrier.) In the following, we shall study this fourth displacement effect and its relation to the other three contributions in more detail.

Of course, the electric field does also influence the wave packet after tunneling through the barrier, but this does not change the tunneling probability – unless the wave packet is “pulled” back into the barrier again. This case is

relevant for scenarios where the time-averaged potential approximation applies, but it will not play a role here. One should also stress that the above dissection according to the various stages of the temporal evolution (or the spatial regions) is not sharp as we are dealing with wave-packets instead of point particles. Due to the corresponding uncertainty, all these phenomena will be intertwined in general. Only in appropriate limiting cases, it will be possible to separate these effects clearly, as we shall see below.

II. KRAMERS-HENNEBERGER MAP

The fourth displacement effect described above can be nicely understood using the Kramers-Henneberger transformation [10] which describes an exact mapping of a purely time-dependent electric field to the induced quiver motion $\chi(t)$. In order to briefly recapitulate the basic principle, let us start from the Schrödinger equation

$$i\partial_t\psi = -\frac{[\nabla - iq\mathbf{A}(t)]^2}{2m}\psi + V\psi. \quad (2)$$

For a purely time-dependent vector potential $\mathbf{A}(t)$, we may eliminate the quadratic term $q^2\mathbf{A}^2/(2m)$ by a global phase transformation $\psi \rightarrow e^{i\phi(t)}\psi$ with $\dot{\phi} = q^2\mathbf{A}^2/(2m)$.

If we now consider a Galilei transformation $\mathbf{r} \rightarrow \mathbf{r} + \mathbf{v}t$ which changes the time derivative as $\partial_t \rightarrow \partial_t - \mathbf{v} \cdot \nabla$, we see that the additional term is equivalent to a constant vector potential \mathbf{A} proportional to the velocity \mathbf{v} . This identification also works for time-dependent vector potentials $\mathbf{A}(t)$ which can thus be represented by the displacement $\mathbf{r} \rightarrow \mathbf{r} + \chi(t)$ given by

$$\dot{\chi}(t) = -\frac{q\mathbf{A}(t)}{m}, \quad (3)$$

which is precisely the classical solution of a point particle with mass m and charge q in the electric field generated by the vector potential $\mathbf{A}(t)$. Thus, the vector potential $\mathbf{A}(t)$ can be translated into a corresponding displacement $\chi(t)$ of the wave-function ψ .

III. RECTANGULAR POTENTIAL

In order to study the four effects (pre-acceleration, energy mixing, potential deformation, and displacement) mentioned in the Introduction, let us start with the extremely simple case of a rectangular (box) potential of height V_0 and length L in one dimension

$$V(x) = V_0\Theta(x)\Theta(L-x). \quad (4)$$

In the absence of the vector potential $A(t)$, we would have an incident wave with energy E_{in} on the left-hand side $x < 0$ of the potential, plus a reflected wave with the same energy E_{in} . Including the vector potential $A(t)$ changes the incident wave according to the Kramers-Henneberger

transformation described above, while the reflected wave will in general contain a mixture of different energies E . Thus we arrive at the general ansatz

$$\psi(t, x < 0) = e^{-iE_{\text{in}}t + i\sqrt{2mE_{\text{in}}}[x - \chi(t)]_+} + \int dE \psi_{\text{ref}}(E) e^{-iEt - i\sqrt{2mE}[x - \chi(t)]}. \quad (5)$$

The term $\sqrt{2mE_{\text{in}}}\chi(t)$ in the exponent of the first line describes the acceleration by the electric field before hitting the barrier. Similarly, we use the general ansatz for the solutions inside the barrier

$$\psi(t, 0 < x < L) = \int dE e^{-iEt} \times \left(\psi_{\text{int}}^+(E) e^{+\sqrt{2m(V_0-E)}[x - \chi(t)]_+} + \psi_{\text{int}}^-(E) e^{-\sqrt{2m(V_0-E)}[x - \chi(t)]} \right), \quad (6)$$

as well as the transmitted solutions

$$\psi(t, x > L) = \int dE \psi_{\text{tra}}(E) e^{-iEt + i\sqrt{2mE}[x - \chi(t)]}, \quad (7)$$

where we have assumed that there is no wave incident from the right-hand side of the barrier $x > L$.

Now the matching conditions for $\psi(t, x)$ and $\psi'(t, x)$ at $x = 0$ and $x = L$ for all times t uniquely determine $\psi_{\text{ref}}(E)$, $\psi_{\text{int}}^\pm(E)$, and $\psi_{\text{tra}}(E)$. While the resulting set of equations is linear and thus solvable via numerical discretization, for example, we shall use some analytical approximations to gain further insight in the following.

A. Sudden approximation

As our first example, let us consider a very strong and short pulse $A(t)$ which can be approximated by a Dirac delta function $A(t) \propto \delta(t)$. According to Eq. (3), this corresponds to a sudden displacement $\chi(t) = \Delta\chi\Theta(t)$, where we assume $L > \Delta\chi > 0$. Considering an initially stationary solution with E_{in} , we find two major effects:

At the front of the barrier (around $x = 0$), the displaced wave function is no longer an energy eigenstate, implying a mixture of energies E . The contributions corresponding to higher energies $E > E_{\text{in}}$ can then tunnel through the barrier more easily than the initial stationary solution with E_{in} .

At the rear of the barrier (around $x = L$), a part of the exponential tunneling tail with length $\Delta\chi$ is “pushed” out of the barrier and thus the probability density behind the barrier is exponentially enhanced by a factor of $e^{2\sqrt{2m(V_0-E_{\text{in}})}\Delta\chi}$, which could be quite large.

B. Opaque-barrier approximation

In order to treat more realistic time-dependences $\chi(t)$, we employ the opaque-barrier (low-energy) approximation. To this end, we assume that the potential height

V_0 is much larger than all other energy and frequency scales, such as $V_0 \gg E_{\text{in}}$. Furthermore, we assume that the barrier width L is also much larger than all other length scales, such as $L \gg |\chi|$. As a result, the tunneling rate is strongly suppressed due to $\sqrt{2mV_0}L \gg 1$, i.e., the barrier is very opaque (see also [11]).

In addition to the large quantity $\sqrt{2mV_0}L \gg 1$, we only keep those terms where an energy $E \ll V_0$ is combined with the long length L as well as those terms where the displacement $\chi \ll L$ is combined with the large barrier height V_0 . To be consistent, we neglect all terms which do not contain a large quantity (V_0 or L), such as all combinations of an energy $E \ll V_0$ with a displacement $\chi \ll L$. Within this scheme, the acceleration before the barrier $\sqrt{2mE_{\text{in}}}\chi(t)$ in Eq. (5) is neglected.

Using this approximation scheme, we may simplify the matching conditions at $x = 0$ and $x = L$. Due to the exponential suppression of the tunneling rate, we have $\psi_{\text{int}}^+(E) \ll \psi_{\text{int}}^-(E)$ such that the contribution from $\psi_{\text{int}}^+(E)$ can be neglected at $x = 0$. To leading order in E/V_0 , we then find $\psi_{\text{ref}}(E) \approx -\delta(E - E_{\text{in}})$ which yields

$$\psi_{\text{int}}^-(E) \approx -2i\sqrt{\frac{E_{\text{in}}}{V_0}} \int \frac{dt}{2\pi} e^{i(E-E_{\text{in}})t - \sqrt{2mV_0}\chi(t)}. \quad (8)$$

Consistent with the simple picture described in the previous Section III A, this equation describes the energy mixing at the front of the barrier $x = 0$ due to the time-dependent displacement $\chi(t)$. Then we may use the remaining matching condition at $x = L$ in order to determine the transmitted solution

$$\psi_{\text{tra}}(E) \approx \psi_E^0 \int \frac{dt}{2\pi} e^{i(E-E_{\text{in}})t - \sqrt{2mV_0}[\chi(t+i\mathfrak{T}) - \chi(t)]}, \quad (9)$$

where $\psi_E^0 = 4e^{-\sqrt{2mV_0}L + E_{\text{in}}\mathfrak{T} - i\sqrt{2mE}L} \sqrt{E_{\text{in}}/V_0}$ collects the χ -independent factors and \mathfrak{T} denotes the Büttiker-Landauer traversal time [11] for this case (with $V_0 \gg E_{\text{in}}$)

$$\mathfrak{T} = L\sqrt{\frac{m}{2V_0}}. \quad (10)$$

Note that the first two exponentials $e^{-\sqrt{2mV_0}L + E_{\text{in}}\mathfrak{T}}$ in ψ_E^0 are the leading-order contributions of the undisturbed tunneling exponent $e^{-\sqrt{2m(V_0 - E_{\text{in}})}L}$.

C. Dynamically assisted tunneling

The result (9) now enables us to study the enhancement of tunneling due to the vector potential $A(t)$. In this form (9), we directly see the invariance under Galilei and gauge transformations $A(t) \rightarrow A(t) + \text{const}$. Furthermore, it is interesting to note that the exponent $\sqrt{2mV_0}[\chi(t+i\mathfrak{T}) - \chi(t)]$ is consistent with the change of the instanton action [12]

$$\sqrt{2mV_0}[\chi(t+i\mathfrak{T}) - \chi(t)] = -\sqrt{\frac{2V_0}{m}} \int_t^{t+i\mathfrak{T}} dt' qA(t'), \quad (11)$$

because $\sqrt{2V_0/m}$ is the undisturbed instanton velocity. Thus, the above Eq. (11) is the analogue to formula (10) in [13]. However, that work [13] was mainly focused on the tunneling exponent, whereas the above Eq. (9) does also contain the pre-factor [for the box potential (4) and within the used approximations].

If we derive the typical energy gain or loss from Eq. (9) via the saddle-point method

$$\begin{aligned} \Delta E = E - E_{\text{in}} &\approx -i\sqrt{2mV_0}[\dot{\chi}(t+i\mathfrak{T}) - \dot{\chi}(t)] \\ &= iq\sqrt{\frac{2V_0}{m}}[A(t+i\mathfrak{T}) - A(t)], \end{aligned} \quad (12)$$

we also find agreement with the instanton picture [12]. Note that the real time t corresponds to the rear $x = L$ of the barrier, the complex time $t+i\mathfrak{T}$ to the front $x = 0$, see also [14].

As expected, the time scale distinguishing the adiabatic from the non-adiabatic (impulse) regime is the Büttiker-Landauer traversal time (10).

In the adiabatic regime of slowly varying $\chi(t)$, the difference $\chi(t+i\mathfrak{T}) - \chi(t) \approx i\mathfrak{T}\dot{\chi}(t)$, is purely imaginary. Thus, the main effect is an energy shift ΔE given by $mL\dot{\chi}(t)$, i.e., the energy gained in the electric field. A real contribution $\sqrt{2mV_0}\mathfrak{T}^2\ddot{\chi}(t)/2$ to the exponent in Eq. (9) arises to second order in \mathfrak{T} . This contribution can be re-written as $\mathfrak{T}\Delta E/2$ and just reflects the quasi-static deformation of the potential by the electric field.

In the non-adiabatic regime of rapidly changing $\chi(t)$, however, we may get a stronger enhancement of the tunneling probability – as expected from the previous considerations. The first term $\chi(t+i\mathfrak{T})$ in the exponent in Eq. (9) stems from the front end $x_{\text{in}}^E = 0$ of the barrier where the imaginary shift $t \rightarrow t+i\mathfrak{T}$ to complex time corresponds to energy mixing. The second term $\chi(t)$ stems from the rear end $x_{\text{out}}^E = L$ and reflects how the wavefunction is “pushed” out of the barrier. Altogether, we obtain the following rough estimate for the enhancement of the tunneling probability

$$\mathcal{P}_\chi \sim \mathcal{P}_0 \exp \left\{ \mathcal{O} \left(2\sqrt{2mV_0}\Delta\chi \right) \right\}. \quad (13)$$

Note, however, that the simple result (9) has been derived for the box potential (4) and will not apply to other potential barriers $V(x)$ in general. The discontinuities at the front $x_{\text{in}}^E = 0$ and the rear end $x_{\text{out}}^E = L$ make the energy mixing and displacement mechanisms quite efficient – this may change for other $V(x)$.

IV. TRIANGULAR POTENTIAL

In order to study the difference between a very steep potential slope and a more gradual change, let us consider a triangular potential

$$V(x) = \frac{x}{L} V_0 \Theta(x) \Theta(L-x). \quad (14)$$

Of course, the ansatz for the solutions outside the barrier is the same as before in Eqs. (5) and (7). The solutions

inside the barrier can be written in terms of displaced Airy functions Ai and Bi

$$\begin{aligned} \psi(t, 0 < x < L) = & \int dE e^{-iEt+i\varphi(t)} \times \\ & \left(\psi_{\text{int}}^{\text{A}}(E) \text{Ai} \left[\left(\frac{2mV_0}{L} \right)^{1/3} \left(x - \chi(t) - \frac{EL}{V_0} \right) \right] + \right. \\ & \left. + \psi_{\text{int}}^{\text{B}}(E) \text{Bi} \left[\left(\frac{2mV_0}{L} \right)^{1/3} \left(x - \chi(t) - \frac{EL}{V_0} \right) \right] \right), \quad (15) \end{aligned}$$

with the additional global phase $\varphi(t) = V_0\chi(t)/L$, since an x displacement of a linear potential $V(x) \propto x$ translates into a variation of the potential height.

As before, we apply the opaque-barrier and low-energy approximation $\chi(t) \ll L$ and $E \ll V_0$. In addition, the slope V_0/L of the triangle is assumed to be small such that $V_0\chi(t)/L \ll E$. Under these assumptions, products of small terms are neglected. Note that this includes the above phase $\varphi(t)$ as it scales with the product of the small slope V_0/L and $\chi(t)$. However, as this phase $\varphi(t)$ does also include a time integral over $\chi(t)$, neglecting $\varphi(t)$ poses a restriction on the relevant time scales, which should not be too long. This is consistent with our previous considerations, as we are interested in rapid (i.e., non-adiabatic) changes.

Then, in analogy to the opaque-barrier approximation for the box potential, we find $\psi_{\text{int}}^{\text{A}}(E) \gg \psi_{\text{int}}^{\text{B}}(E)$. Using the approximations described above, we find the transmitted solution

$$\psi_{\text{tra}}(E) \approx \psi_E^0 \int \frac{dt}{2\pi} e^{i(E-E_{\text{in}})t + \sqrt{2mV_0}\chi(t)}. \quad (16)$$

where ψ_E^0 now describes the undisturbed ($\chi = 0$) amplitude for the triangle (14).

Comparing Eqs. (9) and (16), we find that the term $\chi(t + i\mathfrak{T})$ describing the energy mixing at the front end is missing – just the “pushing out” effect at the rear end $x = L$ of the barrier remains. The suppression of energy mixing at the front end $x_{\text{in}}^E = EL/V_0$ of the barrier (i.e., the first classical turning point) can intuitively be understood by the nearly adiabatic evolution in space and time induced by the gradual change (with a very small slope).

To complete the picture, let us consider the case of a triangular potential turned around, where the step-like discontinuity is at the front end while we have the gradual change at the rear end. As one might have expected from the previous considerations, we now obtain “the other half” of Eq. (9), i.e., the term $\chi(t + i\mathfrak{T})$ describing the mixing of energies at the front end – while the “pushing out” effect at the rear end has negligible effect due to the nearly adiabatic evolution in space and time induced by the gradual change.

Depending on the temporal structure of $\chi(t)$, the energy mixing $\chi(t + i\mathfrak{T})$ and the “pushing out” contribution $\chi(t)$ can be very different. For example, enhancing the tunneling probability by “pushing out” part of the wave-function obviously requires $\chi > 0$, while the

energy mixing contribution $\chi(t + i\mathfrak{T})$ can also enhance tunneling if the electric field points in the other direction – provided that its temporal structure (e.g., spectrum) contains large enough frequency components.

In stationary tunneling, one cannot observe such a difference between the triangular potential (14) and its mirror image. Due to unitarity, the tunneling probability does not depend on whether the wave is incident from left or right. The time-dependent vector potential $A(t)$, however, induces a non-equilibrium situation, where such a breaking of symmetry is possible. This phenomenon is closely related to quantum ratchets, see, e.g., [15].

V. EXPERIMENTAL REALIZATIONS

Since tunneling plays a role in various areas of physics, its dynamical assistance could be observed in several scenarios. However, as most of them will not correspond to a rectangular or shallow triangular potential, let us first briefly discuss the case of a general potential $V(x)$.

A. Büttiker-Landauer traversal time

For general potentials $V(x)$, the Büttiker-Landauer traversal time \mathfrak{T} is given by [11]

$$\mathfrak{T} = -\frac{d\mathfrak{S}_E}{dE} = \int_{x_{\text{in}}^E}^{x_{\text{out}}^E} dx \sqrt{\frac{m}{2[V(x) - E]}}. \quad (17)$$

This quantity plays a manifold role. It describes the (imaginary) propagation time of an instanton from x_{in}^E to x_{out}^E . Furthermore, it measures how much the instanton action \mathfrak{S}_E (which determines the tunneling exponent) decreases when increasing the energy E . As a consequence, the Büttiker-Landauer traversal time \mathfrak{T} provides an estimate for the frequency components ω a pulse (or time-dependent field) should contain to facilitate a significant enhancement of tunneling. If the characteristic frequency components ω are too low $\omega\mathfrak{T} \ll 1$, the energy mixing is not sufficient to shift the instanton action \mathfrak{S}_E enough. As a result, the Büttiker-Landauer traversal time \mathfrak{T} can be used to separate slow (adiabatic) from fast (non-adiabatic) processes.

Note, however, that this quantity \mathfrak{T} does not yield any information about the efficiency of the energy mixing or “pushing out” processes. For example, \mathfrak{T} does not depend on whether the particle is incident from left or right, cf. Sec. IV. The Büttiker-Landauer traversal time \mathfrak{T} corresponds to the change of the tunneling exponent, but does not describe the pre-factor in front of the exponential. In the Floquet-picture, for example, these pre-factors are determined by the matrix elements between the Floquet bands, which determine the efficiency of the energy mixing or “pushing out” processes.

It should also be stressed here that the Büttiker-Landauer traversal time \mathfrak{T} is not necessarily the unique answer to the question of how long the particle stays inside the barrier during tunneling – this is indeed a non-trivial issue (already at the stage of a proper definition, see also [16, 17]). Instead, it is an important quantity for discriminating slow from fast processes, as explained above. In this role, it provides a good first estimate of the experimental requirements for observing assisted tunneling. From Eq. (17), we may read off the rough scaling law $\mathfrak{T} = \mathcal{O}(L\sqrt{m/[V-E]})$ where L is again the length of the barrier. In analogy, the instanton action \mathfrak{S}_E in Eq. (1) can be estimated via $\mathfrak{S}_E = \mathcal{O}(L\sqrt{m[V-E]})$. Now, since \mathfrak{S}_E should not be too large in order to have a measurable tunneling probability, we obtain the rough order-of-magnitude estimate $\mathfrak{T} \sim \mathcal{O}(L^2m)$.

B. Ultra-cold atoms in optical lattices

On a comparably large length scale of order micrometer, optical lattices generated by standing laser beams in the optical or near-optical regime provide a potential landscape for ultra-cold atoms in which they can tunnel from one potential minimum to the next one, see, e.g., [2]. The potential barrier height can be tuned by the laser strength (and its detuning). The above estimate $\mathfrak{T} \sim \mathcal{O}(L^2m)$ of the Büttiker-Landauer traversal time scales as the inverse of the recoil energy $E_R = k^2/(2m)$ which is typically of the order of tens of kHz. Non-adiabatic variations should then be in the sub-millisecond regime, which is not beyond the experimental capabilities. An effective electric field can be generated by accelerated motion of the optical lattice (i.e., a real displacement in space), which can be understood as an inverse of the Kramers-Henneberger transformation. This realization allows us to study dynamically assisted tunneling for neutral particles such as atoms.

C. Electrons in solids

Another prototypical example are electrons in solid-state devices with characteristic length scales between the nanometer and the micrometer scale. By fabricating these devices and applying gate voltages, one could even appropriately realize a box (4) or triangular (14) potential. Due to the smaller length scales and the smaller (effective) mass of the electron, the Büttiker-Landauer traversal time is much shorter in this case and corresponds to frequencies ranging from the tera-Hertz to the infra-red regime which can be coupled in via real electromagnetic fields.

D. Atomic physics

On even smaller length scales in the nanometer or sub-nanometer regime, electrons tunnel from one atomic or molecular orbital to another or into free space (field ionization). The reduction of the characteristic length scales goes along with a further increase of the typical frequency scales necessary to reach the non-adiabatic regime, which range from the optical or near-optical frequencies up to the keV regime for tightly bound electrons around highly charged (high- Z) nuclei.

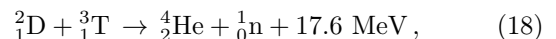
E. Nuclear α -decay

Tunneling on yet smaller length scales in the picometer to femtometer regime plays an important role in nuclear physics. As one of the first applications of quantum tunneling, Georg Gamov explained the Geiger-Nuttall law of nuclear α -decay [4] via tunneling of the α -particle through the Coulomb barrier of the remaining nucleus [3]. Of course, it would be interesting to study the option for dynamically assisting this process, for example with the strong field generated by an x-ray free-electron laser (XFEL). This topic has induced several, partly controversial, discussions in recent years, see, e.g., [18, 19].

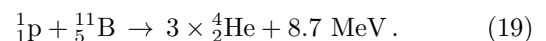
Following our strategy above, let us estimate the Büttiker-Landauer traversal time for this case. As shown in [20], for example, the associated frequency scales are in the 100 keV to MeV regime, see also [19]. Even though the mass of the α -particle is much larger than the electron mass, the extremely small length scales lead to ultra-short times. Since frequencies in the 100 keV to MeV regime are probably hard to reach with current or near-future XFEL facilities, one should search for alternatives. One such option for creating short enough pulses could be the electromagnetic field generated by an additional nucleus (see also [21]) with an energy of order 50 MeV passing by at a distance of order 10^2 femtometer. Of course, this electromagnetic field is not really spatially homogeneous – but the main effects should persist, at least qualitatively.

VI. NUCLEAR FUSION

In the following, let us study nuclear fusion in more detail [13, 22–24], which can be regarded as the process opposite to nuclear α -decay (or, more general, nuclear fission). Interesting examples include deuterium-tritium



or proton-boron fusion (see, e.g., [25])



First, we focus on the most simple case of two particles with masses m_1 and m_2 and charges q_1 and q_2 in the

initial state. Later we shall discuss the generalization to more complicated scenarios such as muon-assisted fusion.

A. The model

Describing the two nuclei as non-relativistic point particles (in the low-energy regime), their dynamics is governed by the two-body Lagrangian

$$L_{12} = \frac{m_1}{2} \dot{\mathbf{r}}_1^2 + \frac{m_2}{2} \dot{\mathbf{r}}_2^2 - V(|\mathbf{r}_1 - \mathbf{r}_2|) + (q_1 \dot{\mathbf{r}}_1 + q_2 \dot{\mathbf{r}}_2) \cdot \mathbf{A}(t), \quad (20)$$

where the potential $V(|\mathbf{r}_1 - \mathbf{r}_2|)$ contains the Coulomb repulsion at large distances and the nuclear attraction at short distances. The vector potential \mathbf{A} represents the field of the XFEL, which can be approximated by a purely time-dependent field because the XFEL wavelength is much larger than the characteristic length scales of our problem, see also [13].

In center-of-mass $\mathbf{R} = (m_1 \mathbf{r}_1 + m_2 \mathbf{r}_2)/(m_1 + m_2)$ and relative coordinates $\mathbf{r} = \mathbf{r}_1 - \mathbf{r}_2$, the effective single-body Lagrangian for the latter reads

$$L = \frac{m}{2} \dot{\mathbf{r}}^2 - V(|\mathbf{r}|) + q_{\text{eff}} \dot{\mathbf{r}} \cdot \mathbf{A}(t), \quad (21)$$

with the reduced mass $1/m = 1/m_1 + 1/m_2$ and the effective charge $q_{\text{eff}} = (q_1 m_2 - q_2 m_1)/(m_1 + m_2)$. Upon quantization, we arrive at the same Schrödinger equation (2), but with re-scaled variables m and q_{eff} .

B. Scaling analysis

In order to identify the relevant parameters, let us first perform a scaling analysis of the Schrödinger equation (2) which is facilitated by the self-similarity of the Coulomb potential. Neglecting the details of the nuclear attraction at short distances (in a low-energy approximation), the potential $V(|\mathbf{r}|)$ is a homogeneous function of degree -1 , i.e., $V(|\lambda \mathbf{r}|) = V(|\mathbf{r}|)/\lambda$. This allows us to cast the Schrödinger equation (2) into a dimension-less form. Using the initial energy E in order to set the frequency and time scale, the length scale can be set by the outer (classical) turning point r_E where $V(r_E) = E$. Then the comparison of the kinetic term $\nabla^2 \psi / (2m)$ with the energy $E\psi$ yields the first dimension-less parameter

$$\eta = 2mEr_E^2 = \frac{2m}{E} \left(\frac{q_1 q_2}{4\pi\epsilon_0} \right)^2. \quad (22)$$

The square root of this parameter yields the undisturbed WKB tunneling exponent $\mathcal{P} \sim \exp\{-\pi\sqrt{\eta}\}$ in Eq. (1) and the Büttiker-Landauer traversal time $E\mathcal{T} = \pi\sqrt{\eta}/4$ for this potential. As explained above, this WKB tunneling exponent (and thus η) should not become too large in order to have a measurable tunneling probability.

The second dimension-less parameter can be constructed by incorporating the remaining term $q_{\text{eff}}\mathbf{A}$ in

the Schrödinger equation (2). Of course, in view of the dimension-less parameters (22) and E/ω , this construction is not unique. Motivated by the above considerations, we choose to compare the amplitude of the displacement (3) with r_E giving

$$\zeta = \frac{q_{\text{eff}} A}{m\omega r_E} = \frac{q_{\text{eff}} A}{mc} \frac{E}{\omega} \frac{4\pi\epsilon_0 c}{q_1 q_2}, \quad (23)$$

where the last ratio on the right-hand-side is the inverse of the QED fine-structure constant modified by the charge numbers Z_1 and Z_2 of the two nuclei. The first ratio is analogous to the inverse Keldysh parameter $1/\gamma$ or the laser parameter a_0 , but now with the electron mass being replaced by the reduced mass of the nuclei. Hence, this quantity ζ will typically be smaller than unity – but again it should not be too small to see a significant effect.

The fact that the two dimension-less parameters η and ζ in Eqs. (22) and (23) should not be too far above or below unity, respectively, shows that we do not have good scale separation in our problem – which makes it hard to distinguish the four effects (pre-acceleration, energy mixing, potential deformation, and displacement) mentioned in the Introduction. Instead, they will all be intertwined. Still, the previous results, especially the comparison between the rectangular and the triangular potential, suggest that energy mixing may be less efficient than displacement, for example, due to the gradual change of the Coulomb potential at the outer turning point r_E .

As another lesson, we may compare deuterium-tritium with proton-boron fusion by means of the above scaling analysis. For the proton-boron system, the Coulomb strength $\propto q_1 q_2$ is a factor of five stronger than in the deuterium-tritium case, while the reduced mass is roughly a factor of 3/4 smaller. According to Eq. (22), the energy should thus be nearly a factor of twenty larger in order to achieve the same WKB tunneling probability. Note, however, that this rough estimate is based on neglecting the details of the nuclear attraction, i.e., the real factor will be a bit smaller than twenty. Nevertheless, as the effective charge q_{eff} of the proton-boron system is approximately a factor of 5/2 larger than in the deuterium-tritium case, the required vector potentials do not differ much (only by a factor of 3/2) in the two cases.

C. Numerical results

As explained above, the analytical scaling analysis in the previous section does not take into account the fact that the Coulomb potential is cut off at nuclear distances of a few femtometer. In order to include this effect and to arrive at quantitative results, we solved the one-dimensional Schrödinger equation in the presence of the cut-off Coulomb potential $V(x)$ and the time-dependent pulse $A_x(t) = A_0/\cosh^2(\omega t)$ numerically for initial Gaussian wave-packets.

Let us first discuss the case of deuterium-tritium fusion with an effective charge $q_{\text{eff}} \approx q/5$ and reduced mass

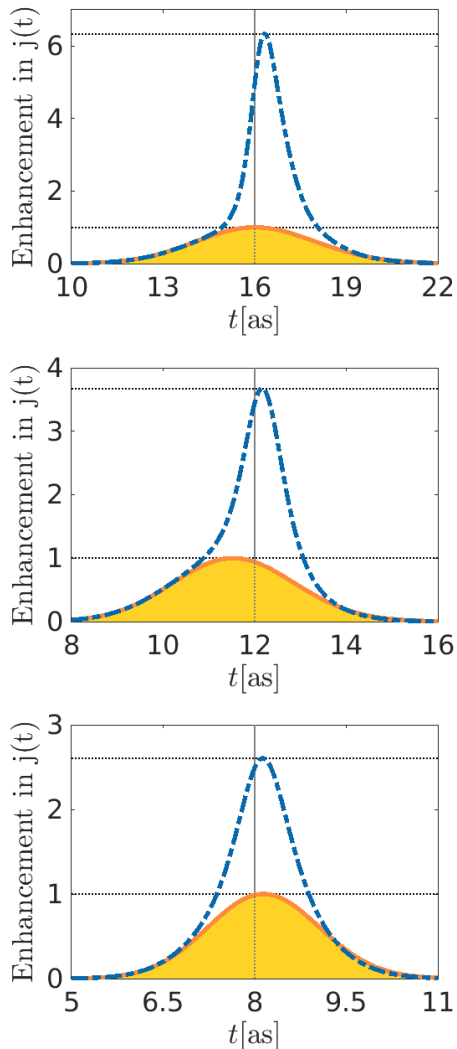


FIG. 1. Enhancement of the tunneling rate for deuterium-tritium fusion with initial kinetic energies of 2 keV (top), 4 keV (middle), and 8 keV (bottom). The orange curves enclosing the yellow bell-shaped regions correspond to the undisturbed tunneling rates $j(t)$ of the initial Gaussian wave-packets without the electric field while the blue dashed-dotted curves show the enhancement due to the pulse $A_x(t)$ with $\omega = 1$ keV and a peak field strength of 10^{16} V/m.

$m \approx 1$ GeV. For initial kinetic energies of 2, 4, and 8 keV, the outer classical turning points r_E determined by the Coulomb repulsion, which correspond to the initial turning points x_{in}^E in Eq. (1), are $r_E \approx 720$ fm, 360 fm, and 180 fm, respectively. The inner turning point, corresponding to x_{out}^E in Eq. (1), is determined by the nuclear attraction and lies around 4 fm.

For these energies (2, 4, and 8 keV), the Büttiker-Landauer traversal times are given by $\mathfrak{T} \approx 2$ as, 0.7 as, and 0.25 as, respectively, while the dimension-less parameters in Eq. (22) assume the values $\eta \approx 60$, 30 and 15, respectively. In view of $\hbar \approx 0.7$ keV as, we see that we may probe non-adiabatic effects with frequencies in the

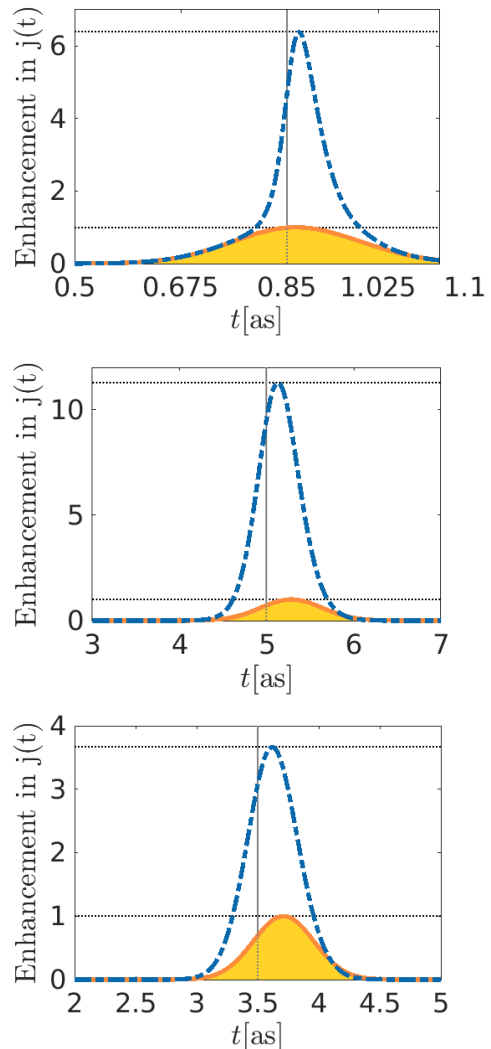


FIG. 2. Enhancement of the tunneling rate for proton-Boron fusion. The top plot corresponds to an initial kinetic energy of 38 keV and a pulse with $\omega = 19$ keV and 28×10^{16} V/m, which represents the scaling transformation of the scenario in Fig. 1 (top). For comparison, using the same pulse with $\omega = 1$ keV and 10^{16} V/m as in Fig. 1 for deuterium-tritium fusion does also yield significant enhancement for initial kinetic energies of 40 keV (middle) and 80 keV (bottom).

keV regime.

A pulse $A_x(t)$ with $\omega = 1$ keV and a peak field strength of 10^{16} V/m then corresponds to a Kramers-Henneberger displacement of $\Delta\chi \approx 130$ fm. Hence the dimension-less parameter in Eq. (23) assumes the values $\zeta \approx 0.1$, 0.2, and 0.4 for these energies (2, 4, and 8 keV).

The enhancement of the tunneling rate (defined as the probability current $j(t)$ on the rear end of the barrier) is displayed in Fig. 1. For all three values of the initial kinetic energy (2, 4, and 8 keV), we see that we obtain a significant enhancement whose relative strength decreases a bit with increasing energy. As explained above, the absence of good scale separation makes it hard to

disentangle the four contributions (pre-acceleration, energy mixing, potential deformation, and displacement). However, comparison with the results of Ref. [13] where mainly the tunneling exponent has been considered – see Eq. (10) in that work, which is the analogue of our formula (11) for the box potential – suggests that the energy mixing contribution is suppressed by the gradual change of the Coulomb potential near the outer turning point r_E , which is consistent with our results for the triangular potential.

As motivated by the scaling analysis above, let us compare these results for deuterium-tritium fusion with the proton-Boron scenario. First, in order to obtain approximately the same dimension-less parameters η and ζ as in the deuterium-tritium case with $E = 2$ keV, we choose an initial kinetic energy of $E = 38$ keV and a pulse with $\omega = 19$ keV and 28×10^{16} V/m. The outer classical turning point is then $r_E \approx 190$ fm and the Büttiker-Landauer traversal time $\mathfrak{T} \approx 0.1$ as. Comparing the top plots in Figs. 1 and 2, we indeed find rather good agreement of the relative enhancement rates, even though the inner turning point (a bit above 4 fm for the proton-Boron case) does not follow the scaling transformation.

For comparison, we also considered the impact of the same pulse (with $\omega = 1$ keV and 10^{16} V/m) as in the deuterium-tritium case. As one may observe in Fig. 2 (middle and bottom), such a pulse does also yield significant enhancement rates for initial kinetic energies of 40 and 80 keV. However, in view of the shorter Büttiker-Landauer traversal times $\mathfrak{T} \approx 0.1$ as and 0.03 as, such a pulse with $\omega = 1$ keV may already be too slow to probe non-adiabatic effects.

VII. CONCLUSIONS

We study how tunneling of a charged particle through a static potential barrier $V(x)$ could be dynamically assisted by an additional time-dependent electric field. We identify four main mechanisms corresponding to the stages of the temporal evolution or the spatial regions: (*i*) pre-acceleration before the barrier, (*ii*) energy mixing at its front end, (*iii*) deformation of the potential barrier, and (*iv*) displacement at its rear end. While the two effects (*i*) and (*iii*) are already present in the adiabatic regime of slowly varying electric fields, the other two phenomena (*ii*) and (*iv*) require sufficiently fast – i.e., non-adiabatic – changes of the electric field.

For the special cases of rectangular and triangular potential barriers, we were able to disentangle the four contributions by means of approximate analytic solutions. We found that the two non-adiabatic effects (*ii*) energy mixing and (*iv*) displacement (occurring at the front and rear end, respectively) are dual to each other with the main difference that the former one (*ii*) is associated to an analytic continuation to complex times $t \rightarrow t + i\mathfrak{T}$ where \mathfrak{T} is the Büttiker-Landauer traversal time. This analytic continuation reflects the energy shift,

which in turn changes the tunneling through the barrier.

The occurrence of a complex time is also related to another distinction between the two contributions (*ii*) and (*iv*). The displacement effect (*iv*) strongly depends on the sign of the electric field: In one direction, the electric field would “push” parts of the wave-function out of the rear end of the barrier and thereby enhance tunneling – while an electric field pointing in the opposite direction would “pull” them into the barrier again and thereby suppress tunneling. In contrast, the energy mixing effect (*ii*) can enhance tunneling for both signs of the electric field – especially deep in the non-adiabatic regime, where the shift of the energy induced by the time-dependence of the electric field becomes the most important contribution.

Furthermore, the comparison between the rectangular and the triangular potentials indicates that the efficiency of the two non-adiabatic effects (*ii*) and (*iv*) strongly depends on the shape of the potential at the turning points and is suppressed in the case of a gradual change. This finding is related to the quantum ratchet effect where tunneling in one direction may be favored compared to the other in non-equilibrium situations.

The Büttiker-Landauer traversal time \mathfrak{T} mentioned above is an important quantity in this respect because it can be used to distinguish slow (i.e., adiabatic) from fast (i.e., non-adiabatic) processes. Since tunneling is a crucial effect in many areas of physics, we briefly discuss the observability of the considered mechanisms in several scenarios, such as ultra-cold atoms in optical lattices, electrons in solids and in atoms/molecules, and nuclear α -decay.

Finally, we turn our attention to nuclear fusion and discuss the special scaling properties of this process stemming from the Coulomb potential. As an explicit example, we study a Sauter pulse $A_x(t) = A_0/\cosh^2(\omega t)$ with $\omega = 1$ keV and a peak field strength of 10^{16} V/m and find a significant enhancement of the tunneling rate for deuterium-tritium fusion with initial energies between 2 and 8 keV as well as for proton-Boron fusion in the 40–80 keV energy range.

Of course, the required field strength of 10^{16} V/m is quite large, but still well below the Schwinger critical field $E_S = m_e^2 c^3 / (q\hbar) \approx 1.3 \times 10^{18}$ V/m. Even though it is probably beyond the present capabilities of x-ray free-electron lasers (XFEL), such field strengths might be achievable with further technological progress, e.g., focusing the XFEL beam better. Another interesting option could be high-harmonic focusing [26] or similar effects of light-matter interaction at ultra-high intensities. As a different approach, such ultra-short and ultra-strong pulses (though with a potentially non-negligible spatial dependence) could be generated by charged particles (such as α particles) with sufficiently high energies (e.g., 50 keV or above) and small enough impact parameters (e.g., 500 fm or below).

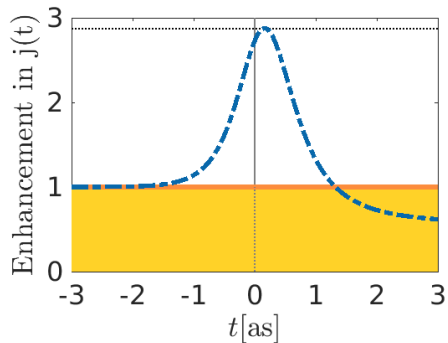


FIG. 3. Enhancement of the tunneling rate starting in a bound state as a toy model for muon-assisted deuterium-tritium fusion, again a pulse with $\omega = 1$ keV and 10^{16} V/m has been assumed.

VIII. OUTLOOK

As became evident from the previous considerations, our understanding is by far not complete yet and there are many ways for further progress. For example, one could generalize the approximate analytical solutions derived above to other potentials, such as combinations of piece-wise constant, linear, or even parabolic potential barriers. Another obvious generalization is the solution of the full 3D-Schrödinger equation, e.g., in position representation or after an expansion into spherical harmonics. Even though one would expect the main mechanisms (such as the displacement) to persist, there should be quantitative differences, e.g., regarding the pre-factors.

This could also pave the way to study the impact of electromagnetic fields $\mathbf{A}(t, \mathbf{r})$ depending on space and time. Related studies of the Sauter-Schwinger effect (see, e.g., [20]) show a non-trivial interplay between the spatial and the temporal dependence of the field. In this respect, it could be interesting to compare the assisted tunneling studied in this work with the dynamically assisted Sauter-Schwinger effect [27] which is governed by a relativistic (Dirac or Klein-Fock-Gordon) wave equation instead of the Schrödinger equation.

A. Muon-assisted fusion

As one can observe in Fig. 1, the relative enhancement of the tunneling rate does – in stark contrast to the tunneling rate itself – not depend very strongly on the initial kinetic energy, which is consistent with the expected behavior of the displacement mechanism, for example. Thus, instead of starting with an asymptotically free scattering state (which was the scenario studied above), one could consider an initial bound state created by a dip in the Coulomb potential. This could be regarded as a toy model for muon-assisted nuclear fusion where the deuterium and tritium nuclei form a bound state with a muon, see, e.g., [28, 29].

Motivated by this toy model, we solved the Schrödinger equation in the presence of the same pulse $A_x(t)$ with $\omega = 1$ keV and 10^{16} V/m as before, but now with a potential $V(x)$ admitting a bound state, which we used as our initial state. The result is plotted in Fig. 3 and shows that such a pulse can also induce a significant enhancement in this case. Even though the potential $V(x)$ is a bit different, one would expect that the displacement mechanism operates in a very similar way, as the vicinity of the inner turning point is basically unchanged. However, the pre-acceleration mechanism should be strongly affected as it acts on the initial state.

Furthermore, it should be stressed here that the case of muon-assisted fusion is much more complex. For example, the electric field does not only couple to the relative motion of the deuterium and tritium nuclei via q_{eff} , it also couples directly to the oppositely charged muon (which is much lighter). Thus we have a real three-body problem here, which is far more involved – but also offers far more interesting possibilities. This includes the eigen-frequencies of the three-body problem which partially also lie in the keV regime and thus facilitate a strong (and possibly resonant) coupling to the external electric field. For a bigger picture, one should reconsider the whole process in the presence of the external electromagnetic (e.g., XFEL) field, including the unwanted sticking of the muon to the produced α -particles, which might also be affected by the external field.

ACKNOWLEDGMENTS

The authors thank N. Ahmadiroz, R. Sauerbrey, G. Torgrimsson, and other colleagues from the HZDR for fruitful discussions. Funded by the Deutsche Forschungsgemeinschaft (DFG, German Research Foundation) – Project-IDs 398912239 and 278162697 – SFB 1242.

-
- [1] Apart from the smallness of Planck's constant \hbar in everyday units, the laws of quantum mechanics, such as the quantum Zeno effect [30], prevent us from directly observing of the process of quantum tunneling. However, sometimes the evanescent tails in more general wave propagation phenomena are considered as analogues to tunneling. These could of course be observed with the naked eye, for example in water waves.
- [2] I. Bloch, *Ultracold quantum gases in optical lattices*, Nature Phys. **1**, 23 (2005).
- [3] G. Gamow, *Zur Quantentheorie des Atomkernes*, Z. Phys. **51**, 204 (1928).
- [4] H. Geiger and J.M. Nuttall, *The ranges of the α particles from various radioactive substances and a relation between range and period of transformation*, Philos. Mag. Ser. 6, **22**, 613 (1911); [Erratum *ibid.* **23**, 439 (1912)].
- [5] As one example, let us mention the recent controversy regarding the dynamical assistance of tunneling in nuclear α -decays, see, e.g., [19] and Sec. V E. Another example is the ongoing discussion about the tunneling time, see, e.g., [16, 17] and Sec. V A.
- [6] S. Coleman, *The uses of instantons*, in *Aspects of symmetry* (Cambridge University Press, 1985).
- [7] M. Grifoni, P. Hänggi, *Driven quantum tunneling*, Phys. Rep. **304**, 229 (1998).
- [8] W. Franz, *Einfluß eines elektrischen Feldes auf eine optische Absorptionskante*, Z. Naturforsch. A **13**, 484 (1958).
- [9] L.V. Keldysh, *The effect of a strong electric field on the optical properties of insulating crystals*, J. Exptl. Theoret. Phys. (U.S.S.R.) **34**, 1138 (1958); [Sov. Phys. JETP **7**, 788 (1958)].
- [10] W.C. Henneberger, *Perturbation Method for Atoms in Intense Light Beams*, Phys. Rev. Lett. **21**, 838 (1968).
- [11] M. Büttiker and R. Landauer, *Traversal Time for Tunneling*, Phys. Rev. Lett. **49**, 1739 (1982).
- [12] More details regarding the applicability of the instanton picture to dynamically assisted tunneling will be postponed to a forthcoming publication.
- [13] F. Queisser and R. Schützhold, *Dynamically assisted nuclear fusion*, Phys. Rev. C **100**, 041601(R) (2019).
- [14] B.I. Ivlev, V.I. Melnikov, *Dramatic stimulation of tunneling by an rf field*, JETP Lett. **41**, 142 (1985); Pis'ma Zh. Eksp. Teor. Fiz. **41**, 116 (1985).
- [15] P. Reimann, M. Grifoni, and P. Hänggi, *Quantum Ratchets*, Phys. Rev. Lett. **79**, 10 (1997).
- [16] R. Ramos, D. Spierings, I. Racicot, A.M. Steinberg, *Measurement of the time spent by a tunnelling atom within the barrier region*, Nature **583**, 529 (2020).
- [17] H.G. Winful, *Tunneling time, the Hartman effect, and superluminality: A proposed resolution of an old paradox*, Phys. Rep. **436**, 1 (2006).
- [18] D.S. Delion and S.A. Ghinescu, *Geiger-Nuttall Law for Nuclei in Strong Electromagnetic Fields*, Phys. Rev. Lett. **119**, 202501 (2017).
- [19] A. Pálffy and S.V. Popruzhenko, *Can Extreme Electromagnetic Fields Accelerate the α Decay of Nuclei?*, Phys. Rev. Lett. **124**, 212505 (2020).
- [20] C. Schneider & R. Schützhold, *Dynamically assisted Sauter-Schwinger effect in inhomogeneous electric fields*, J. High Energ. Phys. **2016**, 164 (2016).
- [21] B. Ivlev and V. Gudkov, *New enhanced tunneling in nuclear processes*, Phys. Rev. C **69**, 037602 (2004).
- [22] W. Lv, H. Duan, and J. Liu, *Enhanced deuterium-tritium fusion cross sections in the presence of strong electromagnetic fields*, Phys. Rev. C **100**, 064610 (2019).
- [23] F. Queisser and R. Schützhold, *Comment on "Enhanced deuterium-tritium fusion cross sections in the presence of strong electromagnetic fields"*, arXiv:2003.02661.
- [24] G. Kälbermann, *Assisted fusion*, arXiv:0910.3447.
- [25] L. Giuffrida et al, *High-current stream of energetic α particles from laser-driven proton-boron fusion*, Phys. Rev. E **101**, 013204 (2020).
- [26] S. Gordienko, A. Pukhov, O. Shorokhov, and T. Baeva, *Coherent Focusing of High Harmonics: A New Way Towards the Extreme Intensities*, Phys. Rev. Lett. **94**, 103903 (2005).
- [27] R. Schützhold, H. Gies and G. Dunne, *Dynamically assisted Schwinger mechanism*, Phys. Rev. Lett. **101**, 130404 (2008).
- [28] F. Frank, *Hypothetical Alternative Energy Sources for the 'Second Meson' Events*, Nature **160**, 525 (1947).
- [29] L.W. Alvarez et al, *Catalysis of Nuclear Reactions by μ Mesons*, Phys. Rev. **105**, 1127 (1957).
- [30] B. Misra and E.C.G. Sudarshan, *The Zeno's paradox in quantum theory*, J. Math. Phys. **18**, 756 (1977).